

Global stability of self-gravitating discs in modified gravity[★]

Neda Ghafourian, Mahmood Roshan[†]

Department of Physics, Ferdowsi University of Mashhad, P.O. Box 1436, Mashhad, Iran

Accepted XXX. Received YYY; in original form ZZZ

ABSTRACT

We study the global stability of a self-gravitating disc in the context of Modified Gravity (MOG) using N-body simulations. This theory is a relativistic scalar-tensor-vector theory of gravity and presented to address the dark matter problem. In the weak field limit MOG possesses two free parameters α and μ_0 which have been already determined using rotation curve data of spiral galaxies. The evolution of a stellar self-gravitating disc and more specifically the bar instability in MOG is investigated and compared to a Newtonian case. Our models have exponential and Mestel-like surface densities as $\Sigma \propto \exp(-r/h)$ and $\Sigma \propto 1/r$. It is found out that, surprisingly, the discs are more stable against the bar mode in MOG than in Newtonian gravity. In other words, the bar growth rate is effectively slower than the Newtonian discs. Also we show that both free parameters, i.e. α and μ_0 , have stabilising effects. In other words, increase in these parameters will decrease the bar growth rate.

Key words: galaxies: kinematics and dynamics– galaxies: spiral– instabilities– galaxies: evolution– cosmology: dark matter

1 INTRODUCTION

Early numerical studies showed that if any flat bulge-less self-gravitating disc of particles is set under equilibrium of centrifugal force and the Newtonian gravitational force, the particles can not maintain their circular motion and in a timescale very short compared with the lifetime of the spiral galaxies, the disc is heated up and its overall configuration changes from a flat disc to a stellar bar, for example see Miller et al (1970); Hohl (1971). This means that the disc is globally unstable. This fact is known as the bar instability in the literature.

To tackle this problem Ostriker & Peebles (1973) in their pioneering paper showed that by adding a spherical rigid component to the system, the evolution of the initial disc to the final bar could be controlled. In fact for the first time in the literature they introduced the dark matter halo concept. Historically, the global stability of the disc galaxies played a key role among the astrophysicists to accept that the dark matter problem, which had already alarmed by Zwicky (1933), is a serious one and it is not due to the lacks in observational equipment. For a comprehensive review of the subject we refer the reader to Sanders (2010).

After Ostriker & Peebles pioneer work, several analytical and numerical studies have been done to investigate the role of the dark matter halo in the evolution of spiral galaxies, for example see Sellwood (1981); Efstathiou et al (1982); Athanassoula & Selwood (1986); Athanassoula (2002) and Sellwood (2014) for a review of the subject.

It is well understood that dark matter halo stabilises the disc against global perturbations and slows down the growth rate of the stellar bar. On the other hand, it should be noted that about 65% of luminous spiral galaxies are barred (Sheth et al 2008). The presence of bars in the real galactic discs is much larger than traditionally thought. This fraction is a function of the cosmic redshift z , and is smaller at larger redshifts. For example it drops to 20% at $z = 0.8$ (Sheth et al 2008). This means that stellar bars have been effectively formed in the spiral galaxies during the past 7 Gyr. Furthermore, bars exhibit interesting features and play important roles in the evolution of the disc galaxies. They seem to be linked to some engrossing phenomena like secular evolution and pseudo-bulge growth (Kormendy & Kennicutt 2004) and galactic rings (Buta & Combes 1996). Furthermore, bars are key ingredients that help to redistribute angular momentum between different components of disc galaxies (Athanassoula 2002). They are also thought to excite spiral arms (Toomre 1969; Sanders & Huntley 1976). They transport gas to the centre of disc galaxies and may trigger AGN activity. Therefore it is necessary to emphasise that

[★] By modified gravity we mean a scalar-tensor-vector gravity known as MOG in the literature.

[†] E-mail: mroshan@um.ac.ir

the dark matter halo is needed to slow down the bar growth and not to totally suppress it.

It is clear that fate and dynamics of stellar bars closely depend on the properties of the dark matter halos. In other words, the bar growth is directly related to the dark matter problem. More specifically, dark matter halos not only moderate the bar instability but also are necessary to explain the flat rotation curves of the spiral galaxies. However dark matter particles have not yet been discovered while there are several laboratories which look for these exotic particles using direct and indirect techniques, see [Bertone et al \(2010\)](#). This fact keeps open another approach to the problem: i.e. modified gravity. These theories are widely used to address the dark energy (for example see [Capozziello & De Laurentis 2011](#) for a review of dark energy models) and the dark matter problem (for example see [Milgrom 1983](#) and [Famaey & McGaugh 2012](#) for modified Newtonian dynamics (MOND) , [Moffat 2006](#) for Modified Gravity (MOG) and [Burrage et al 2016](#) for a symmetron-like non-minimally coupled scalar-tensor theory).

Among the modified theories presented to resolve the dark matter problem, MOND (and its corresponding relativistic theory TeVeS; [Bekenstein 2004](#)) is one of the most successful theories. The global stability of spiral galaxies in MOND has been investigated in [Christodoulou \(1991\)](#); [Brada & Milgrom \(1999\)](#) and [Tiret & Combes \(2007\)](#) using N-body simulations. It is found in [Christodoulou \(1991\)](#) and [Brada & Milgrom \(1999\)](#) that disc galaxies are more stable in MOND than in Newtonian gravity. [Tiret & Combes \(2007\)](#) showed that although the bar instability occurs sooner in MOND than in Newtonian gravity, stellar bar weaken in MOND while in the dark matter halo model they continue to grow.

In this paper, we study the bar instability in MOG using N-body simulations. One may naturally expect that the stability of the spiral galaxies should be explained in this theory without any need to dark matter halos. In the weak field limit, MOG is able to fit a large number of galaxy rotation curve data [Brownstein & Moffat \(2006a\)](#), as well as the X-ray galaxy clusters data [Brownstein & Moffat \(2006b\)](#) without any need of non baryonic matter. Recently it has been claimed in [Israel & Moffat \(2016\)](#) that MOG has the potential to explain merging cluster dynamics, such as Bullet Cluster and Train Wreck Cluster, without dark matter. For some cosmological consequences of this theory, we refer the reader to [Moffat & Toth \(2009\)](#); [Moffat \(2015\)](#); [Roshan \(2015\)](#) and [Jamali & Roshan \(2016\)](#). Furthermore, the local stability of disc galaxies in MOG has been already investigated in [Roshan & Abbassi \(2015\)](#) and the generalised Toomre criterion has been derived. Also for some N-body and numerical studies on the dynamics of disc galaxies in MOG see [Brandao & de Araujo \(2010\)](#) and references therein.

The outline of this paper is as follows: In section 2 we briefly discuss the weak field limit of MOG. In section 3 we set up the initial conditions and describe the simulation. Results for the exponential model $\Sigma \propto e^{-r/h}$ has been presented in section 4. We have done some tests on the reliability of the results in the section 5. In this section we have also presented the results of the stability analysis of the Mestel-like disc. Conclusions are drawn in section 6.

2 WEAK FIELD LIMIT OF MOG

MOG is a fully relativistic and covariant generalisation of General Relativity (GR). Despite GR which is a tensor gravity, MOG is a scalar-tensor-vector theory of gravity in which additional to the metric tensor there are two scalar fields, $\mu(x^\beta)$ and $G(x^\beta)$, and also a massive Proca vector field ϕ^β . These extra degrees of freedom enable MOG to explain some astrophysical data related to the dark matter problem. In order to study the dynamics of a disc galaxy, we need the weak field limit of this theory. Therefore let us briefly review MOG's modified Poisson equations. Perturbing the above mentioned fields around their background values and substituting them into the field equations, one can find the modified Poisson equations, for details see [Moffat & Rahvar \(2013\)](#); [Moffat & Rahvar \(2014\)](#); [Roshan & Abbassi \(2014\)](#). The equations of motion of spinning and non-spinning test particles in MOG has been investigated in [Roshan \(2013\)](#).

In the weak field limit, the test particle's equation of motion is

$$\frac{d^2 r}{dt^2} = -\nabla\Phi \quad (1)$$

where Φ is an effective gravitational potential defined as

$$\Phi = \Psi + \chi\phi^0 \quad (2)$$

in which ϕ^0 is the zeroth component of the vector field, χ is a coupling constant, and Ψ and ϕ^0 satisfy the following differential equations

$$\nabla^2\Psi = 4\pi(1 + \alpha)G\rho \quad (3)$$

$$(\nabla^2 - \mu_0^2)\chi\phi^0 = -4\pi\alpha G\rho \quad (4)$$

where χ and α are related as $\alpha = \frac{\chi^2}{\omega_0 G}$. Also μ_0 is the background value of the scalar fields μ and appears as a free parameter, ω_0 is a coupling constant, G is the gravitational constant, and ρ is the matter density. It is necessary to mention that MOG possesses two coupling constants ω_0 and χ in its generic action. However in the weak field limit these coupling constants join and form a single free parameter α . Observational values of the free parameters α and μ_0 obtained from rotation curve data of spiral galaxies are 8.89 ± 0.34 and $0.042 \pm 0.004 \text{ kpc}^{-1}$ respectively [Moffat & Rahvar \(2013\)](#). Using equations (3) and (4), the generalised Poisson equation would be

$$\nabla^2\Phi(r) = 4\pi G\rho + \alpha\mu_0^2 G \int \frac{e^{-\mu_0|r-r'|}}{|r-r'|} \rho(r') d^3x' \quad (5)$$

We can simply say that our purpose in this paper is to study the effects of the last term in the right hand side of equation (5) on the global stability of disc galaxies. Using equation (5) for a massive test particle, the acceleration law and the gravitational potential can be written as

$$\ddot{r} = -\frac{GM}{r^2} [1 + \alpha - \alpha(1 + \mu_0 r)e^{-\mu_0 r}] \quad (6)$$

$$\Phi(r) = -\frac{GM}{r} [1 + \alpha - \alpha e^{-\mu_0 r}]. \quad (7)$$

it is clear that by setting to zero α or μ_0 , one can recover the Newtonian gravity. Also since the free parameters are

positive, it is easy to show that MOG leads to stronger force than the Newtonian case. In fact this is a necessary feature for theories which try to address the dark matter problem.

3 GLOBAL STABILITY OF AN EXPONENTIAL DISC IN MOG

In this section we create an initial axi-symmetric disc model with surface density proportional to $\exp(-R/h)$ in Newtonian gravity as well as in MOG. Then we explore their dynamics using an N-body code and concentrate on the bar instability and the growth rate of the stellar bar. For simplicity, our disc model in Newtonian gravity does not possess a dark matter halo; we will call it a "bare" disc model hereafter. This fact will help to compare these theories more clearly. In this sense, this paper follows a same approach as in [Ostriker & Peebles \(1973\)](#), where a bare disc model has been compared with a model in which the gravitational force is modified because of a rigid spherical component. Of course it will be also instructive to compare MOG disc with a more realistic disc model including the dark matter halo [Ghafourian & Roshan \(2017\)](#).

Let us first introduce two main parameters which will help us to quantify the bar instability in the above mentioned disc models.

3.1 Stability parameter β

In galactic simulations there is a common parameter to study the stability of the system. For a virialized system we have $T = \frac{1}{2}|W|$, where T is the total kinetic energy and W is the gravitational potential energy of the system. The total kinetic energy can be decomposed as $T = T_{\text{rot}} + T_{\text{ran}}$. Where T_{rot} is the total rotational kinetic energy of the particles and T_{ran} is the total kinetic energy associated to the random motions of the particles.

It is common to define a stability parameter as $t = \frac{T_{\text{rot}}}{|W|} > 0$. Using the Virial theorem one may show that t is always smaller than $\frac{1}{2}$. If this parameter decreases with time then the random motions of the system will increase. This can be considered as the outset of the instability. In this paper we use another parameter constructed from t as

$$\beta = \frac{1}{2t} - 1. \quad (8)$$

In this case it is easy to show that $\beta = \frac{T_{\text{ran}}}{T_{\text{rot}}}$. It is apparent that a decrease in the ratio of rotational motions to random motions, make t parameter to shrink and β to grow. Since a bar is a pressure dominated configuration, its formation will increase the β parameter. Therefore, this parameter will help to control and interpret the bar instability. Albeit one need to be careful when using this parameter. In fact a growing β does not necessarily mean that a bar mode, $m = 2$, is growing. In principle this parameter can also grow even when there is no excited non-axisymmetric perturbation, $m \neq 0$, in the system. For example when a spherical bulge ($m = 0$) forms in a simulation, β can in principle increase with time. In other words, although β provides a practical tool for exploring the instability, it does not distinguish between different modes of perturbations.

Therefore let us introduce other stability parameters

which measure the growth rate of a given mode m . In this case describing the instability will be more reliable and straightforward.

3.2 Bar strength and Fourier decomposition

Various methods have been used to quantify the bar strength. For example [Athanasoula \(2003\)](#) states that, in a relatively closed system, the ability of the bar to transfer angular momentum to other galactic components determines the strength of the bar. According to [Bournaud & Combes \(2002\)](#), in a relatively open system, bar growth and destruction is linked to the external gas accretion and tidal interactions. Since our disc is an isolated stellar disc, we will study the rate of angular momentum transfer from inner part of the disc to the outer parts in order to quantify the bar strength.

Another way to study the bar strength, is the Fourier intensity amplitude which actually does not specify how influential the bar is on its environment, but determines the brightness of the bar in contrast to its background. However it could be considered as a measure of bar strength [Combes & Sanders 1981](#) and [Elmegreen & Elmegreen 1985](#). In this method the various components of the Fourier expansion are calculated, then the ratio of m th component to the 0th component determines the strength of the m th mode. Another way to find the Fourier components, is to consider the position of the particles in the disc and expand the instantaneous distribution of disc particles as

$$A_m(t) = \sum_j \mu_j e^{im\phi_j} \quad (9)$$

in this case the amplitude a_m is written as (for example see [Sellwood 2016](#))

$$a_m(t) = \left| \sum_j \mu_j e^{im\phi_j} \right|. \quad (10)$$

where μ_j is the mass and ϕ_j is the cylindrical polar angle of each particle. We use this last method in this paper. These parameters are calculated at each time step to determine the amplitude of each mode as a function of time. So the bar strength, for which $m = 2$, would be obtained by the ratio $\frac{a_2}{a_0}$.

The $m = 2$ term of the expansion (9) gives the phase and amplitude of the bar as follows

$$A_2(t) = a_2 e^{2i\phi(t)} \quad (11)$$

Therefore we can simply calculate the angular displacement of the bar, $\phi(t)$ in each time step. Furthermore, we calculate the time derivative, $\dot{\phi}(t) = \Delta\phi/\Delta t$ in each time step. Finally we fit a tenth degree polynomial to the consecutive data points. We mention that $\phi(t)$ is the pattern speed of the bar, i.e. $\Omega_p(t) = \dot{\phi}(t)$.

3.3 Initial conditions

We have modified the standard N-body code presented in [Aarseth \(1985, 1994, 2003\)](#) in order to study MOG effects on the disc dynamics. The original code assumes a Newtonian gravitational force between particles and uses a predictor-corrector method in which every particle is advanced in time

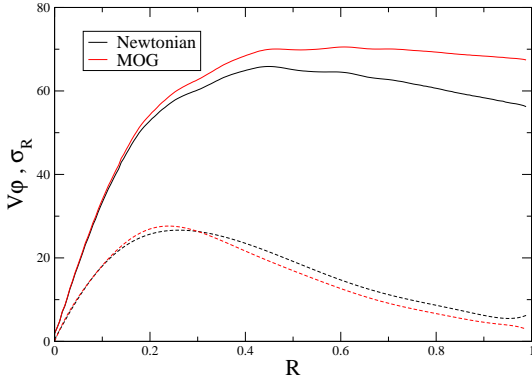


Figure 1. Initial rotational velocities for Newtonian and MOG exponential models. After about $R = 0.1$, velocities in MOG gets higher than the Newtonian case. Dashed curves show the corresponding radial dispersion velocities.

with its own time step $\Delta t_i = (\eta f / \ddot{f})^{1/2}$, where η is an accuracy parameter which affects the value of calculated individual time step of each particle, considered to be $\eta = 0.02$ in our calculations, and f, \ddot{f} are the total force acting on the i th particle and its second derivative respectively. For more details we refer the reader to Aarseth (2003).

Working in the cylindrical coordinate system (r, ϕ, z) , we choose the initial surface density of particles to vary as $\Sigma \propto \exp(-R/h)$ in a disc with initial radius r_0 . Also we choose the units such that $G = 1$, for simplicity we assume an equal mass for all particles and scale it to unity, i.e. $m = 1$. Also we adopt r_0 as our length unit. Therefore we use $R = r/r_0$ as the dimensionless length. In this case the initial radius of the disc is $R_0 = 1$. Albeit for ignoring the singularities that would show up from the close encounters of the particles during the numerical computations, the smoothing parameter ϵ should be included in the definition of the dimensionless length. Therefore in this paper by R we mean

$$R = \sqrt{\left(\frac{r}{r_0}\right)^2 + \epsilon^2} \quad (12)$$

In our main simulations, the value of ϵ is considered to be $\epsilon = 0.05$. Furthermore, we use a dimensionless time $\tau = t/t_0$ in which t_0 is a characteristic time defined in the item 4). Thus, using these units and equation (6), the magnitude of the dimensionless force between two particles takes the form

$$f(R) = \frac{1}{R^2} [1 + \alpha - \alpha(1 + \mu R)e^{-\mu R}] \quad (13)$$

and μ is a dimensionless parameter defined as $\mu = \mu_0 r_0$. We set the initial conditions using a similar procedure presented in Ostriker & Peebles (1973). Let us briefly describe this procedure:

1) In the case of Mestel-like disc, for initial positions we distribute N particles on a disc of radius $R_0 = 1$. In order to set a Mestel-like surface density, we divide the disc into $N/10$ ring and into ten equally spaced slices ($\Delta\phi = 36^\circ$). Then we place one particle in a random position within each cell. The resulting surface density is $\Sigma = N/2\pi R$.

On the other hand, in the case of the exponential disc $\Sigma \propto e^{-R/h}$ with the dimensionless scale length h , we have distributed N particles on a disc with initial radius $R_0 = 1$ using a different procedure presented in Aarseth (2003) (see

chapter 8). We set h to 0.2 in our simulations. Changing this parameter would not change the main results. On the other hand, it is important mentioning that the typical scale length for spiral galaxies is $\sim 2\text{kpc}$, see Binney & Tremaine (2008), and thus our choice is reasonable.

2) For adjusting the initial velocities, every particle is given an initial azimuthal velocity needed to balance with the centrifugal force and hold the particles in the circular orbits. For doing this, each particle is virtually rotated on a circle with radius equal to particle's distance from the centre of the disc and the quantity $\sqrt{-R_i \cdot f_i}$ is computed every 1° . f_i is the force acting on the given particle when it is settled at the position r_i . The average value of these 360 numbers is taken as the initial azimuthal velocity of each particle. The average value of this velocity for each ring is plotted in Fig. 1 for both Newtonian and the MOGian disc. As expected, the rotation curve in MOG is higher than the Newtonian disc.

3) For making the disc stable against local perturbations at $\tau = 0$, the velocity dispersions are added in three directions to each particle using the Toomre criterion and the epicycle approximation. We recall that Toomre criterion is, (Toomre 1964)

$$Q = \frac{\kappa \sigma_R}{3.36 G \Sigma} > 1 \quad (14)$$

where κ is the epicyclic frequency and σ_R is the dispersion velocity in the radial direction. We can rewrite this criterion as $\sigma_R > \sigma_{\min}$ where σ_{\min} is the minimum value of the radial dispersion velocity required for the local stability and is given by $\sigma_{\min} = 3.36 G \Sigma / \kappa$. On the other hand, from epicycle approximation we have a relation between the dispersion velocities as, see Ostriker & Peebles (1973) for more details

$$\frac{\sigma_\phi^2}{\sigma_R^2} \simeq \frac{1}{2} \left(1 + \frac{d \ln v(R)}{d \ln R} \right) \quad (15)$$

where σ_ϕ is the tangential velocity dispersion and $v(R)$ is the circular velocity. Therefore we may write

$$\sigma_{\min} \simeq \frac{\sigma N \Delta}{v(R) \sqrt{1 + \frac{d \ln v(R)}{d \ln R}}} \quad (16)$$

$$\sigma_\phi \simeq \frac{\sigma}{\sqrt{2}} \frac{N \Delta}{v(R)} \quad (17)$$

where $\Delta = 1$ for the Mestel disc and for the exponential disc we have

$$\Delta = \frac{R e^{-R/h}}{h(h - (1 + h)e^{-1/h})} \quad (18)$$

also $\sigma = 0.378$. Setting the initial σ_R to be 20% larger than the minimum value, we have $\sigma = 0.454$. We use this parameter, i.e. σ , in order to control the response of the system to local perturbations.

One should note that the Toomre criterion in MOG is different from (14). In fact generalised version of this criterion in MOG can be written as $\sigma_R > \sigma_{\text{MOG}}$ where $\sigma_{\text{MOG}} > \sigma_{\min}$, for more details see Roshan & Abbassi (2015). However because of the above mentioned 20% enhancement, the difference between the local stability criteria in MOG and Newtonian gravity does not matter, and consequently both models are locally stable. Also the thickness of the disc in the

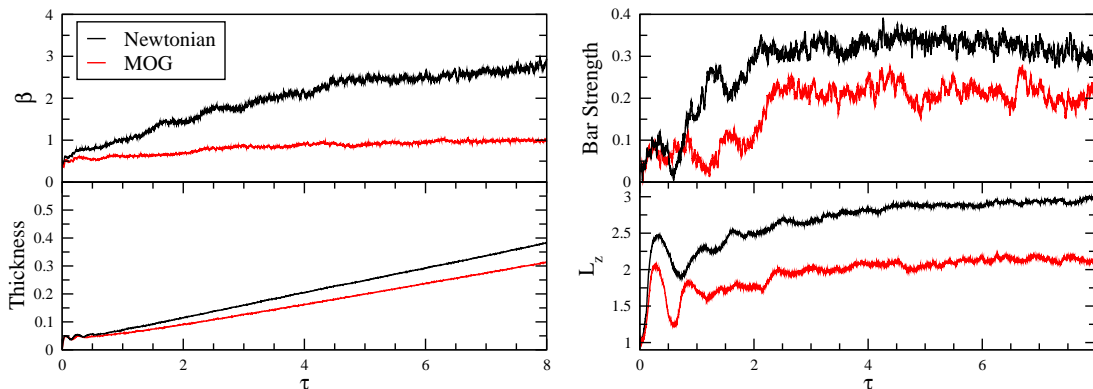


Figure 2. The top left panel shows the time evolution of the β parameter in both models. The bottom left panel demonstrates the thickness of the discs with respect to time. The top right panel shows the bar amplitude in both models. The bottom right panel shows the vertical component of the total angular momentum in the outer part of the disc with inner radius $R = 0.7$.

z direction can be taken into account by adding a velocity dispersion in the vertical direction as $\sigma_z = \sigma_\phi$.

4) Finally, after adding the velocity dispersions, we should re-establish the equilibrium between the gravitational and the centrifugal forces. To do so, the average velocity v of each ring is multiplied by a factor to make it equal with the average velocity of ring before adding the velocity dispersions.

Indeed, the time evolution of the disc is described in terms of the initial average rotation period t_0 of the outer ring and the disc is initially rotating in the counterclockwise direction. The Number of particles is set to $N = 2500$ for the main simulation and has been increased to 10000 in order to check the effects of number of particles, N , on the results. In fact, although our results are also unaltered for particle numbers over 10000, we have not included them, since the error in relative energy conservation gets higher than 1%

It is necessary to mention that the code computes direct summation of the forces over all particle pairs. We have used this method since modifying the gravitational force in the code is straightforward in this case. But the computation time scales as N^2 and makes the code inefficient for large N . Therefore we restrict ourselves to $N \leq 10000$. However we believe that although N is small, it is enough to fulfil our simple purpose in this paper. In other words, we are interested on the overall effects of MOG on the global stability of self-gravitating discs and not on the details of its time evolution. Consequently it does not seem necessary to use large N in the simulation. For a paper with a similar aim in which a similar code is used we refer to Christodoulou (1991) where $N \leq 1200$. Of course to have a more precise view on the evolution of a galactic disc in MOG, it is necessary to employ higher number of particles in the codes which use different methods for computing the gravitational force Ghafourian & Roshan (2017).

It is helpful here to reiterate that Ostriker & Peebles (1973) used simulations with only $N = 150$ to 500 and for the first time showed that rigid halos have stabilizing effects on the self-gravitating discs. Their result has been not ruled out in simulations containing rigid halos and large number of particles N . From this perspective, and considering the limitations of the code and keeping in mind the main aim of the paper, we have restricted ourselves to $N \leq 10000$. However, in

section 5 we have applied three tests to the code in order to check the reliability of the results. More specifically, in the case of Mestel-like disc we present an analytic description which confirms the results obtained from our simulations.

The initial rotational velocity of both Newtonian and MOG models is plotted in Fig. 1. As it is expected, in large distances from the centre the rotation curve in MOGian disc is almost flat and tangibly higher than the Newtonian disc. On the other hand, until about $R = 0.1$, the velocities in both models are equal. In fact in real spiral galaxies MOG modifications to the gravitational law give larger accelerations to the stars and so increases their rotational velocity. Furthermore, σ_R for MOG model is larger than the Newtonian case for $0.1 \lesssim R \lesssim 0.31$ and after $R \sim 0.31$ gets smaller. In fact a same value for the Toomre parameter has been used in both models therefore we can write $(\sigma_R \kappa)_N = (\sigma_{RK})_{\text{MOG}}$. On the other hand, one may show that epicycle frequency in MOG is smaller than the Newtonian model in the interval $0.1 \lesssim R \lesssim 0.31$ and then gets larger. Consequently one may simply explain the behaviour of the radial velocity dispersion in both theories. Albeit one may expect that the epicycle frequency in MOG to be larger than the Newtonian case in any radius since MOG leads to stronger gravitational attraction and consequently increases the epicycle frequency, i.e. $\kappa \propto \sqrt{F(R)}$, where $F(R)$ is the magnitude of the gravitational force. However, one should note that the first derivative of the force with respect to radius is also important for magnitude of κ as

$$\kappa(R) = \sqrt{\frac{dF}{dR} + \frac{3}{R}F(R)} \quad (19)$$

Therefore increasing the strength of the force does not necessarily mean that κ has been increased. In the case of an infinite Mestel disc we have found the exact form of the rotation curve, see equation (A3) in the appendix. One may easily use equation (A3) and compare κ in both theories.

It is necessary to mention that in order to determine the dynamical properties of our models, we need a well-defined centre among the particles about which to perform the simulations. The centre of our N-body system wanders from the centre of our coordinate system. In fact the centre of mass of the system in principle has a non-zero initial velocity. Consequently the centre will move during the simulation and may cause non-real effects and numeric artefacts. We use a

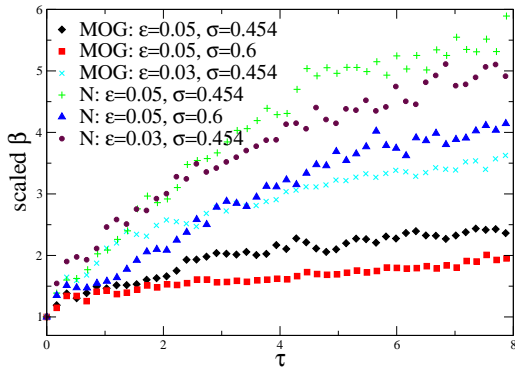


Figure 3. Stability parameter β for different values of ϵ and σ . β is scaled to its initial value at $\tau = 0$. Therefore all curves start from 1.

simple procedure to find the centroid of the system. For each time step, we calculate the Fourier amplitudes with respect to an origin (x_0, y_0) initially chosen near the main origin of the coordinate system, and change this point smoothly until find a point for which the amplitude of the first Fourier mode $m = 1$ is minimum. The final centroid (x_0, y_0) has been shown by a red plus in Fig. 4 for different τ .

As a final remark, the change in total energy can be monitored at regular time intervals in order to measure the global error. In other words, we measure the relative energy conservation $|\Delta E|/E_0$ in each time step. Where E is the total energy of the particles and E_0 is its initial value at $\tau = 0$. In our main simulations this quantity is always lower than 1%.

4 RESULTS

4.1 Stability parameter β

As mentioned above, one useful criterion to check the stability of the discs is the time evolution of β parameter. This parameter measures the ratio of the random motions to rotational motions. Ostriker & Peebles (1973) showed that for a bare disc, this parameter rapidly grows and the disc evolves to a stable pressure dominated configuration, i.e. the stellar bar. On the other hand, β does not grow rapidly in the presence of a rigid halo. As we mentioned before, this fact has been approved in several numerical studies. Regarding our purpose in this paper, it is important to see how fast the disc is evolved to the hot stable state. The time evolution of this parameter in both MOG and Newtonian models has been shown in top left panel of Fig. 2. The initial value of β for MOG disc is slightly smaller than the Newtonian case. This fact is expected since MOG increases the rotational velocity of the particles.

The β parameter in Newtonian disc, as expected, grows rapidly and reaches $\beta \sim 1$ at $\tau \sim 1$, i.e. at the first rotation period. This means that random motions rapidly dominate the disc against the rotational motions. Rapid growth continues until $\tau \sim 4.5$ and after that β grows with a smaller and almost constant slope.

For the MOG disc, it is clear that β parameter raises much slower. It grows to about 0.75 at $\tau = 2.5$, then it grows with an almost constant slope and reaches to about 1. at the end of the simulation. This means that unlike the Newtonian

case, the disc remains approximately rotationally dominated and the bar formation happens with a very small rate compared to the Newtonian disc.

Another quantity for measuring the departures from the initial disc shape, is the thickness of the disc. One may use the root-mean-square value of z of the particles as the thickness of the disc. The time evolution of the thickness has been shown in the bottom right panel of Fig. 2. In Newtonian disc the thickness increases rapidly with time. As mentioned in Ostriker & Peebles (1973), this fact is in agreement with the rapid bar formation. Thickness in the MOG model increases slower.

In order to show that our main results are not sensitive to the magnitude of the softening parameter ϵ , we have performed simulations for different values of ϵ . To see the difference, we have plotted the scaled β parameter, i.e. β/β_0 where β_0 is the initial value of β , in Fig. 3. In the case of Newtonian disc, by comparing the graph of circles ($\epsilon = 0.03$) and pluses ($\epsilon = 0.05$) it is clear that the evolution of the β parameter does not change significantly by changing ϵ . In MOG disc, by comparing the diamonds ($\epsilon = 0.05$) and crosses ($\epsilon = 0.03$), it seems that β parameter in MOG is more sensitive to changes in ϵ than in Newtonian gravity.

4.2 Bar growth

In this subsection we discuss the bar growth in both models. Let us start with the Newtonian disc. The left panel in Fig. 4 shows the time evolution of the Newtonian disc, projected in the equatorial plane. The top left block shows the initial disc. A weak bar starts to form rapidly. The $m = 3$ mode is apparent at $\tau \approx 0.7$ and after $\tau \approx 1$, the bar grows stronger and the spiral arms appear at $\tau \approx 1.4$. They fade and reappear until $\tau \approx 3.3$ but the bar is a permanent feature and stays almost unchanged until the end of the simulation.

In the top right panel in Fig. 2, we have plotted the bar amplitude a_2 . The black curve corresponds to the Newtonian disc. In this case, after experiencing a temporary minimum, the bar amplitude rapidly increases and reaches to 0.27 at 1.2. Then after a temporary decrease, raises again about 0.35 at $\tau = 2$. Then the disc settles in an almost equilibrium state, i.e. the bar. However it is clear that the bar strength decreases with a small slope after $\tau \approx 5$. On the other hand, as we mentioned, the stability parameter β increases smoothly. This means that although the bar is weakened, the random motions are increasing. Therefore one may conclude that the bar decays slowly to a spherical pressure dominated configuration, say a stellar bulge. We checked the existence of this spherical configuration by projecting the positions of the particles in the $z-y$ and $z-x$ planes. Furthermore, we will see in subsection 4.6 that the presence of other modes is tangible compared to the $m = 2$ mode in the first rotation period, specially for $m = 3$. The bar starts to be the dominant mode after $\tau \approx 1$ and reaches its maximum strength at about $\tau \approx 2$.

The red curve in the top right panel in Fig. 2 is the bar amplitude in MOG model. In this case the growth rate is much less than the Newtonian case. More specifically, until $\tau = 2.5$ the $m = 2$ mode forms and decays frequently and the bar strength is weak. In other words, there is an explicit oscillation in the bar amplitude during the first 2.5 rotation periods. It is shown in section 5.1 that these oscillations

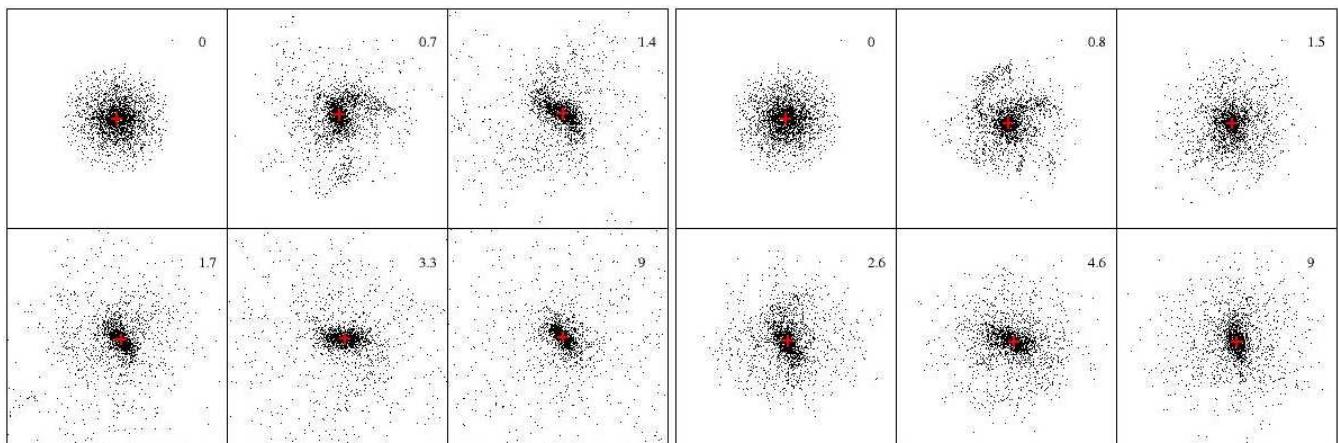


Figure 4. The evolution of the disc with respect to time projected on the x - y plane. The left and right panels belong to the Newtonian and MOG model respectively. Both models are exponential, i.e. $\Sigma \propto e^{-R/h}$.

exist also in the Mestel-like disc. We emphasise that the existence of transient spiral patterns is not the case in the Newtonian disc (without halo). However it seems that they are a key feature in the MOG models. These oscillations in the strength might be an indication of the existence of several modes which are beating.

After $\tau = 2.5$, the disc settles into an equilibrium configuration, with bar amplitude relatively constant thereafter, $a_2/a_0 \sim 0.2$. This fact is also different from the Newtonian disc. In fact, constancy of the bar strength shows that, unlike the Newtonian case the bar mode is a stable configuration and does not decay to a spherically symmetric system. In other words, the final state of the MOG disc, is a shortened bar rotating in the plane of the disc.

The transient nature of the spiral patterns in the MOG model signals that the propagation of the stellar density waves and their interaction with the relevant resonances in the context of MOG could be different from the Newtonian gravity. This issue needs more careful studies in order to determine the origin of this interesting feature. However, it is interesting to mention that there are observations which verify that spiral patterns should be short-lived rather than long-lived structures, see [Sellwood \(2011\)](#).

In order to check the dependency of the results to N , we have shown the bar strength for some different values of N in Fig. 5. It illustrates that the bar amplitude evolves in a similar trend for all N . In fact in both Newtonian and MOG discs, the final value of the bar amplitude is somehow independent of N . More specifically, the time averaged value of the bar magnitude in both theories and for different particle numbers is presented in Table 1. The fractional difference δ is defined as

$$\delta = \frac{\langle a_2 \rangle_N - \langle a_2 \rangle_M}{\langle a_2 \rangle_N} \quad (20)$$

where subscript "N" and "M" stand for Newtonian and MOG models respectively, and N should not be confused with particle numbers. This parameter shows that the averaged value of the bar strength in Newtonian cases is higher than the MOG models. Although there seems to be some random change in δ according to different particle numbers, the main feature that the bar strength in MOG is smaller than the Newtonian case is unchanged. The mean value for the aver-

Table 1. Time averaged value of the bar strength over $\tau = 0$ to $\tau = 8$ for MOG and Newtonian models, in both exponential and Mestel-like discs with different number of particles.

Model	N	$\langle a_2 \rangle_M$	$\langle a_2 \rangle_N$	$\delta \times 100$
$\Sigma \propto \exp(-\frac{R}{h})$	1600	0.16	0.25	36.0
	2500	0.17	0.28	39.28
	4000	0.17	0.33	48.48
	6000	0.18	0.26	30.77
	7000	0.18	0.29	37.93
	8000	0.10	0.28	64.29
	9000	0.20	0.30	33.33
10000	0.17	0.30	43.33	
Mean values	-	0.17	0.29	41.38
$\Sigma \propto \frac{1}{R}$	1600	0.17	0.25	32.0
	2500	0.17	0.29	41.38
	4000	0.24	0.28	14.28
	6000	0.24	0.30	20.0
	7000	0.18	0.29	37.93
	8000	0.23	0.30	23.33
	9000	0.24	0.31	22.59
10000	0.19	0.29	34.49	
Mean values	-	0.21	0.29	27.59

aged bar magnitude in Newtonian is 0.29 while this parameter is 0.17 for MOG, which results in a fractional difference $\bar{\Delta} \approx 41.38\%$. Related discussions of the Mestel-like disc will be presented in section 5.1.

It is also interesting to compare the length of the stellar bar in both theories. We have plotted the length of the bar, after fitting a nineteen degree polynomial, in Fig. (6, top panel) for both models. To do so, at each time τ we assume a rectangle with width ~ 0.2 and length ~ 1 around the line $y = \tan \phi(\tau)x$, where $\phi(\tau)$ is the angular displacement of the bar. Then after dividing this rectangle to small elements, the bar length is chosen to be the length at which the number density of the particles is less than 30% of the centre number density. From Fig.(6, top panel), it is apparent that the bar length is longer in the Newtonian model. It grows to about 0.32 at $\tau = 3.4$ and then declines slowly. This behaviour

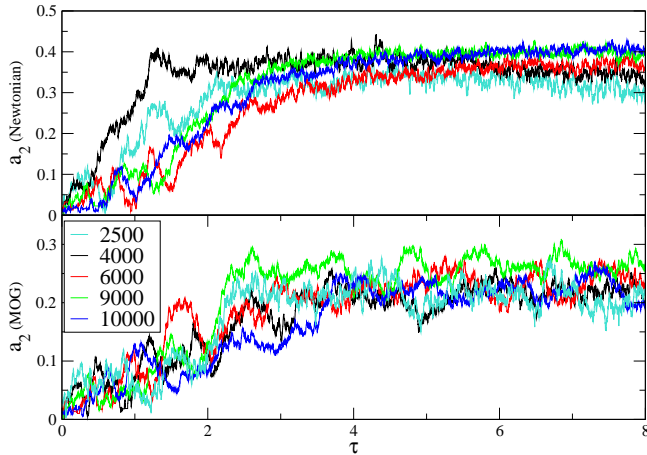


Figure 5. Time evolution of the bar strength for different number of particles N in the disc. For both Newtonian and MOG discs, the final values of the bar strength is somehow independent of N .

is consistent with the bar strength. On the other hand, as expected, the bar length in MOG is shorter. Furthermore, there are obvious oscillations in the bar length in MOG. These oscillations are reminiscent of a similar behaviour in the N-body simulations of the spiral discs in the context of MOND, see Fig. 8 in [Tiret & Combes \(2007\)](#).

The main result of this section is that the final bar strength in MOG is weaker and the growth rate is smaller than the Newtonian case. This result is satisfactory and is what one may expect from a modified theory of gravity. In other words, as we already mentioned, modified gravity has to play a same role as the dark matter halo for suppressing the bar growth rate. However this result seems somehow puzzling. In fact there is no difference between MOG and Newtonian model in the inner disc, and the differences appear at large distances from the centre. On the other hand, the bar is formed in the inner disc. Therefore one may expect that its dynamics would be similar to the Newtonian case. However, as our simulations show, the dynamics of the bar is significantly different in these theories.

4.3 Pattern speed Ω_p

We also calculate the pattern speed $\Omega_p(t)$ using equation (11). The result has been illustrated in Fig. (6, bottom panel) after fitting a nineteenth degree polynomial. Since the bar rotates smoothly, $\Omega_p(t)$ is not as noisy as other functions that we have already plotted. We assume that the pattern exists even in small times. The black curve corresponds to the Newtonian model. In this case the pattern speed rapidly decreases until $\tau \sim 0.25$ and then grows and experience a maximum at $\tau \sim 0.5$. There is another maximum at $\tau \sim 1.8$. After this time, $\Omega_p(t)$ decreases until $\tau = 2.2$ and gets almost constant, i.e. $\Omega_p \sim 8$, until the end of simulations. Albeit there are some small amplitude oscillations.

It is evident that the pattern speed in the MOG model is slightly larger than the Newtonian disc. One may expect this fact since the initial circular velocity of the particles are larger in the MOG model. In this case as in Newtonian model, Ω_p first starts with a decreasing phase. However at around $\tau \sim 0.5$ starts to raise and after experiencing a max-

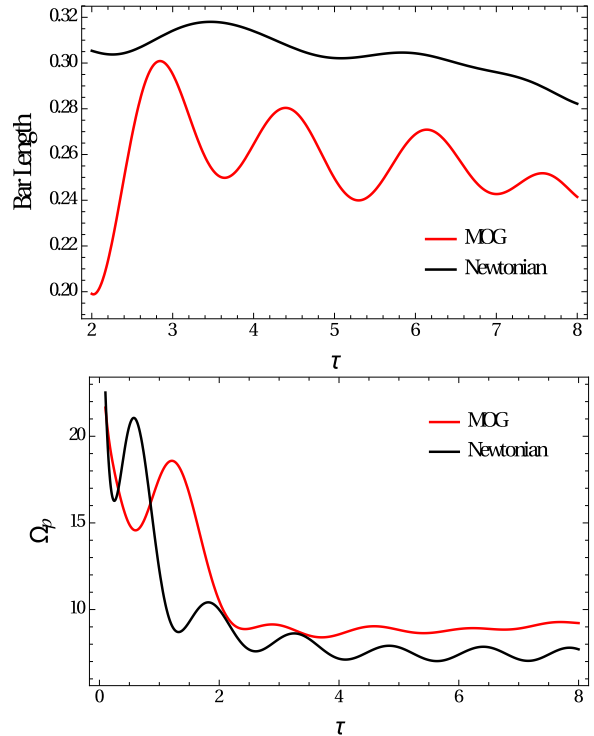


Figure 6. Top panel: the time evolution of the bar length in both exponential models. Since in both models, the bar is fully formed after $\tau \sim 2$, we have plotted its length for $\tau > 2$. Bottom Panel: evolution of the pattern speed with time. The black curve belongs to the Newtonian disc and the red curve is for the MOG model. For very small times, these curves are not reliable since the pattern has been not fully formed at these times.

imum at $\tau \sim 1.3$ starts to decrease and finally reaches the almost constant value $\Omega_p \sim 9$. Existence of maximums in the evolution of the pattern speeds of both models can be simply related to the evolution of the stellar bar. It is clear from Fig. 2 that in the same period of time that the pattern speeds experience a maximum, the bar magnitudes experience a minimum. This means that the stellar bar is temporarily converts its shape to an almost spherical system. Therefore the characteristic size of the pattern gets smaller. Naturally one may expect an increase in the angular momentum of the pattern in this situation. Therefore it is expected that the pattern speed grows in this period of time.

4.4 radial profiles of Σ , v_ϕ and σ_r

It is also instructive to study the radial behaviour of the main quantities like surface density Σ , radial velocity dispersion σ_r and the circular velocity v_ϕ . We have plotted the radial profile of these quantities at different times in Fig. 7. The left and right panels belong to MOG and Newtonian exponential discs respectively. It is clear from top panels that although the rotation curve in both models change with time, the changes are smaller in the MOG model. Moreover, we found that v_ϕ radial profile remains almost unchanged after $\tau \sim 0.4$ in Newtonian model and $\tau \sim 0.7$ in the MOGian disc.

The projected surface density profiles have been plotted in the middle panels. We have scaled Σ to its initial value at

Global stability of self-g

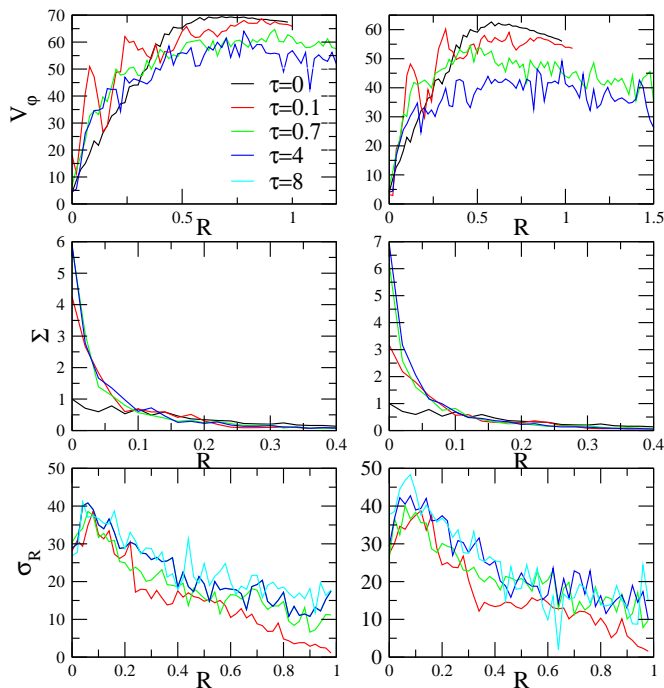


Figure 7. Radial dependency of azimuthal velocity, scaled surface density, and radial velocity dispersion for MOG (left panels) and Newtonian (right panels) at four different times.

$R = 0$. As expected, surface density grows at $R \sim 0$ in both models, and this growth is higher in the Newtonian disc.

In the case of radial dispersion velocities, in the bottom panels, it is clear that in small radii σ_r grows faster in the Newtonian case. More specifically, at $\tau = 8$ the maximum value of σ_r reaches to 48 in the Newtonian disc while it is 15% smaller in the MOGian case.

4.5 Angular momentum exchange

Angular momentum exchange between galactic components is a key factor in the bar formation. Angular momentum exchange plays also a central role for describing many accretion phenomena in astrophysical systems, for example see [Shakura & Sunyaev \(1973\)](#) for viscosity driven angular momentum exchange in accretion discs. In our models, in order to buckle in the centre as a bar, the disc needs to lose angular momentum. For example [Tiret & Combes \(2007\)](#) and [Sellwood \(2016\)](#) has studied the angular momentum transfer from the disc to the surrounding halo during the stellar bar formation. [Sellwood \(2016\)](#) showed that angular momentum transfer from the galactic disc to the live halo, may behave like a source for the bar growth.

Although in our models there is no halo, the angular momentum can be transported throughout the disc by the torques that the stellar bar exerts on the outer parts of the disc. Therefore we checked the angular momentum transfer from inner parts of the disc, to the outer parts. To do so, we have calculated the vertical component of the angular momentum, i.e. L_z , with time for a part of the disc outside the radius $R = 0.7$. The result has been shown in the bottom right panel in Fig. 2. The black and red curves correspond to the Newtonian and MOG models respectively.

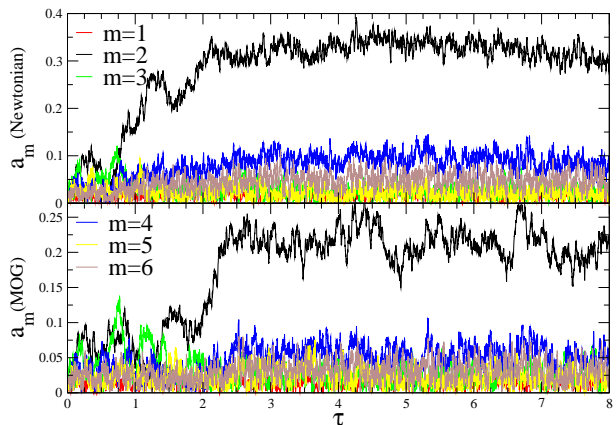


Figure 8. Time evolution of different Fourier modes in a exponential disc for Newtonian and MOG models. The dominant mode for both models is $m = 2$. It is clear that even modes are stronger than the odd modes. The $m = 3$ mode in MOG models is stronger than the Newtonian case.

The angular momentum transport in the Newtonian disc happens with a larger rate. This is expected since the origin for this exchange is the stellar bar, and the bar is stronger in the Newtonian disc and also this bar grows with a faster rate. This difference between the two models can also be obtained using analytic descriptions in the case of Mestel-like disc. The related discussions are included in section 5.1, and calculations are presented in the appendix.

It is interesting to mention that because of the lower azimuthal velocity at larger radii in the Newtonian model, one may expect an opposite behaviour. However, we plotted the surface density of the discs at larger radii in both models, and realized that the surface density of Newtonian Model, is larger than the MOG model at $r \gtrsim 1.1$. This result holds for different times in the evolution of the disc, and means that the spread of the particles to larger distances is higher in the Newtonian model.

4.6 $m \neq 2$ modes

Although from Fig. 4 it is somehow evident that other modes ($m \neq 2$) are not strong enough to dominate the dynamics, we have shown their amplitude, i.e. a_m/a_0 , in Fig. 8. The top panel corresponds to the Newtonian disc and the bottom panel is for the MOG model. In general even modes are stronger than the odd modes. However the dominant mode in both models is the bar mode. In both models, around $\tau \sim 0.7$ there is an explicit enhancement in the amplitude of $m = 3$ mode. In the MOG model this mode even dominates the bar mode for a short period of time. Furthermore, at $\tau \sim 1$ the amplitude of $m = 4$ mode reaches its maximum. It is important to mention that the oscillatory nature of the modes in the MOG is not restricted only to the bar mode and appears for other modes.

4.7 Effects of MOG's free parameters on the bar growth

We recall again that MOG possesses two free parameters, α and μ_0 , in the weak field limit. In principle, these pa-

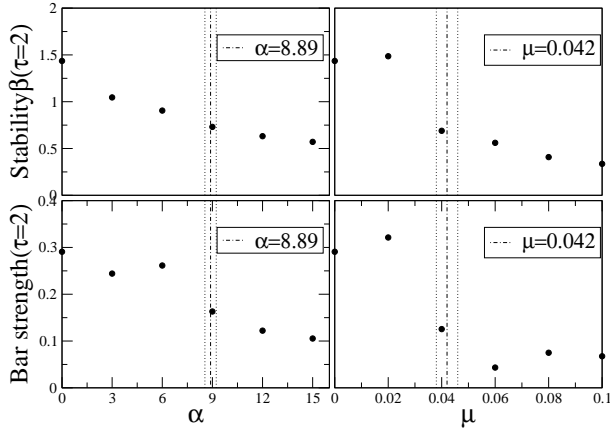


Figure 9. Top left panel shows the β parameter at $\tau = 2$ for a constant μ and different values of α . In the top right panel $\alpha = 8.89$ and β has been computed for different μ . In the bottom panel, with a same procedure, the bar magnitude has been measured at $\tau = 0.5$ for different values of α and μ .

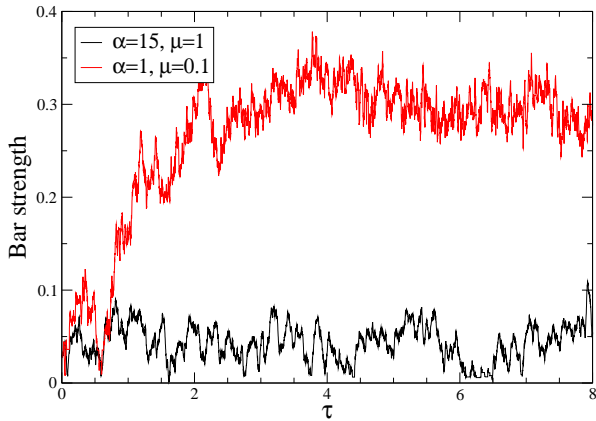


Figure 10. Effect of MOG free parameters on the bar evolution. μ is shown with its scaled value. It is clear that large parameters can totally prevent the bar formation.

parameters are not universal and they may differ from scale to scale (Haghi & Amiri 2016). As we already mentioned, in the case of spiral galaxies, the current observational values for these parameters are $\mu_0 = 0.042 \pm 0.004 \text{ kpc}^{-1}$ and $\alpha = 8.89 \pm 0.34$. In our simulations we have set $\alpha = 8.89$ and $\mu_0 = 0.042 \text{ kpc}^{-1}$. In this section we study the response of the stellar bar to the changes in these free parameters.

To do so, we check the stability parameter β for different values of μ and α . The result has been illustrated in the top panels of Fig. 9. In this figure the observational range of the parameters has been indicated by dot dashed lines. In the top left panel, μ is constant and is set to 0.42 (in its dimensionless form), and the α parameter is varied. The stability parameter has been computed at $\tau = 2$ for different values of α . It is evident that by increasing this parameter β decreases. In other words, by increasing α one may stabilise the disc. At first sight, this result seems somehow bizarre since larger α leads to stronger gravitational force. Consequently one may expect that a stronger gravitational force would destabilise the disc. However we recall that existence of a halo, also

strengthens the radial gravitational force while suppressing the global gravitational instability.

In the top right panel in Fig. 9, we set the α parameter to 8.89 and check the response of the disc to different μ . As in the α parameter case, μ has also stabilising effects on the disc.

Also we have done the same procedure for the bar amplitude and measured it at $\tau = 2$ for different values of the free parameters. The result has been plotted in the bottom panels of Fig. 9. This result also approve the above mentioned point that both free parameters have stabilising effects on the disc. More specifically, large values of free parameters can totally suppress the bar formation, for example see Fig. 10 in which we have compared the bar evolution for small and large values of free parameters. This fact raises the question that if MOG can explain the existence of unbarred galaxies. It is worth mentioning that although the dark matter halo provides a reasonable and satisfactory picture for the bar evolution, it leaves also some unanswered questions. In some cases a halo can even speed up the bar growth, for example see Athanassoula (2002) and Saha & Naab (2013). Recently Sellwood (2016) using N-body simulations found out that angular momentum transfer between a live dark matter halo and the stellar disc can effectively trigger the bar instability. This means that if disc galaxies are assumed to embed in live dark matter halos, then the observational evidence that more than 35% of them lack a strong bar is still a serious challenge.

On the other hand, as we already mentioned, MOG free parameters are not universal constants and have different values in different environments. For example, in Table 1 of Moffat & Rahvar (2013), these parameters are fitted using observational data, and it is shown that for some of the LSB galaxies in their sample, are large and comparable to the values in Fig. 10 for black curve. In other words, in principle, MOG may explain the unbarred galaxies provided that their characteristic values for α and μ are large enough. Therefore, it seems that the special case of unbarred galaxies should be studied more carefully. In other words, it is crucial to find the observational value of the free parameters in these systems and then study their global stability using N-body simulations. We leave this issue as a future study.

In order to find a more reliable method to investigate the effects of these parameters on the evolution of the stellar bar, we have performed several simulations and computed the time average value of β and a_2 during the entire simulation (five rotation periods). The results of β and a_2 have been illustrated in left and right panels of the contour plot Fig. 11 respectively. The upper panels belong to the exponential disc. In the lower panels we have shown the corresponding results for the Mestel-like disc. This figure provides a full parameter space defined by $0 \leq \alpha \leq 15$ and $0 \leq \mu \leq 1$. In fact we have performed 150 simulations, for each model, to cover the parameter space by a symmetric mesh. Albeit by increasing the mesh points and consequently the number of simulation, one may find a better resolution. Contour curves indicate points (α, μ) for which the measured quantity, i.e. $\langle \beta \rangle$ in the right panel and $\langle a_2 \rangle$ in the left panel, are the same. This figure completely approves the results presented in Fig. 9. The left panels in Fig. 11 shows that by increasing the free parameters the bar instability is suppressed more.

The right panels show the averaged bar amplitude. Al-

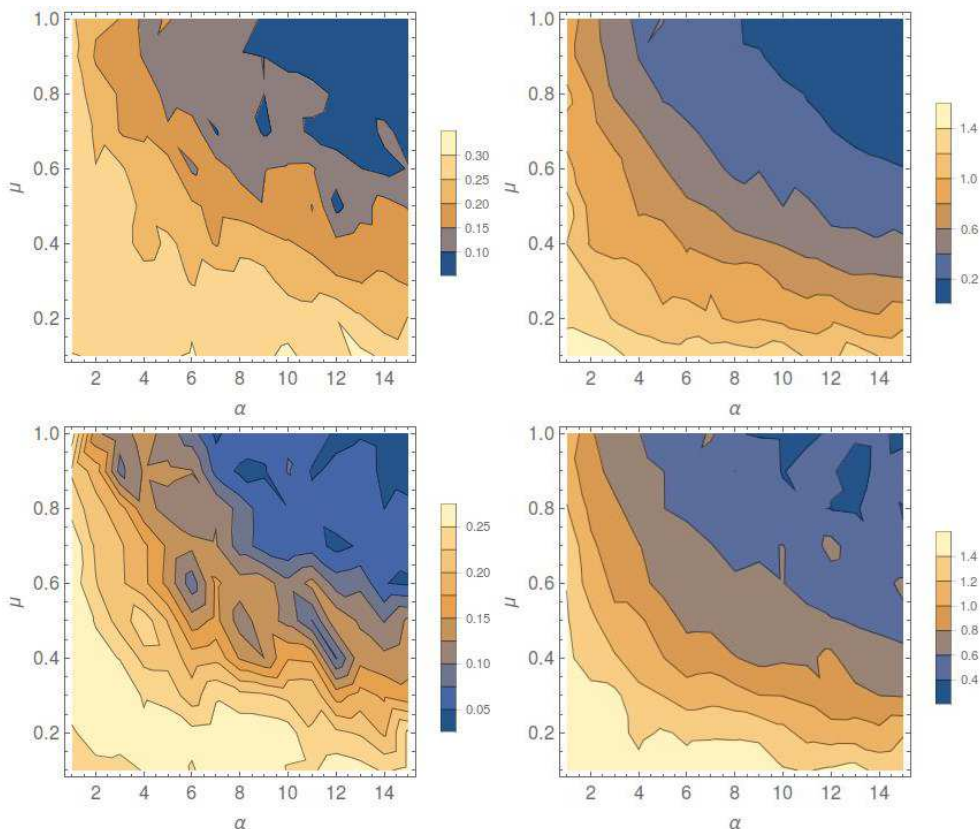


Figure 11. The time averaged value of β has been indicated in the left panel as a contour plot for different values of α and μ . Each point on these panels means a separate simulation, each panel has 150 points. In the right panel the averaged value of the bar amplitude has been computed for different free parameters. Both panels approve that the bar instability is suppressed by increasing the free parameters.

though they are not as smooth as the left panels, specially in the exponential disc, they also show that increasing the free parameters will stabilise the disc. It is clear that the oscillatory nature of the bar amplitude in MOG also appears in this parameter space.

5 TESTS

The limited number of particles in the code is a major concern which made us perform some tests on the reliability of the code. First we applied the code to a Mestel-like disc. Fortunately, in this case we can derive some of the results analytically. As we will show in the next subsection the analytical description confirms our numeric results. As another test, we re-derive the stability criterion introduced by [Efstathiou et al \(1982\)](#) with a different numerical method. And to diminish the possible particle noise, we check our results using a quiet start ([Sellwood 1989](#)).

5.1 Global stability of a Mestel-like disc in MOG

The transfer of angular momentum for a Mestel can be analytically calculated in MOG as well as in Newtonian gravity. Therefore, in order to test our results, we repeated our simulations for a Mestel-like disc, and compared the results with the analytic description. In this section for a Mestel-like disc,

we do the same simulations/analysis that we did for the exponential disc. However, as we will show, the main results does not change and almost all of our analysis and interpretations will also hold for the Mestel-like disc. We recall that although the exponential disc is more realistic, we also study the Mestel-like disc as a toy model, since the transfer of angular momentum for this model is possible to be interpreted analytically in MOG. Therefore, let us briefly present our results for the evolution of the Mestel-like disc. The initial velocities for this disc, in both theories have been plotted in the top left panel in Fig. 12. As expected, the rotation curve in MOG is higher than the Newtonian disc. It is important mentioning that this toy model does not lead to an observationally viable rotation curve.

The bar strength has been plotted in the top middle panel in Fig. 12. The bar starts to form rapidly for both models and in the Newtonian model reaches its maximum amplitude at about $\tau = 1$. The oscillatory nature of the bar is seen again for the MOG model. For this model, the bar continues to grow with a steep slope until about $\tau = 5$ and then continues with an almost constant value. Eventually it is clear that the bar strength in MOG is weaker. More specifically, the mean time averaged value of a_2 in MOG is 0.21 and in Newtonian disc is 0.29. Therefore, the bar magnitude for our Mestel-like model in Newtonian dynamics is about 27.6% larger.

The stability parameter β has been illustrated in the bottom middle panel in Fig. 12. This plot also verifies that

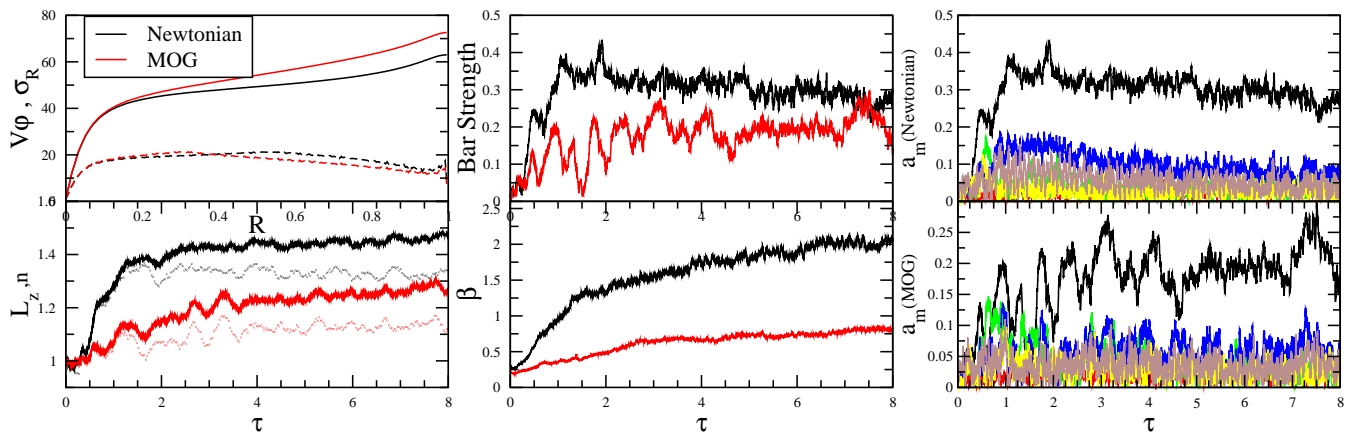


Figure 12. Results for the Mestel-like disc, i.e. $\Sigma \propto \frac{1}{R}$: The top left panel shows the circular velocity in Newtonian gravity and MOG. Of course, this is a toy model and the rotation curve is not consistent with the observations. The dashed curves in this panel are the radial velocity dispersions in both models. The bottom left panel is the vertical component of the total angular momentum of a ring with inner radius $R = 0.7$ in both models. The fractional number of particles, i.e. n , in the outer part of this radius has been indicated by dotted black curve in the Newtonian case and by the dotted red curve for the MOG model. The top middle panel is the bar strength in Newtonian gravity and MOG. The bottom middle panel is the β instability parameter and the right panel is the magnitude of the other Fourier modes, in the same order as in Fig. 8.

the bar instability in Newtonian disc is stronger. It is clear that β does not get larger than 1 at the end of simulation. It was the case also for the exponential disc in MOG. This means that for both models in MOG the random motions do not overcome the rotational motions.

In the right panel in Fig. 12 we have compared other Fourier modes with the bar mode for both theories. The order of the curves is the same as Fig. 8. It is clear that, as in the case of the Mestel-like disc, the bar mode is the most unstable mode in both models. Also the even modes are, in general, stronger than the odd modes. It is also interesting to mention that the $m = 3$ mode is seen for both models during the first orbital period. As we discussed before, appearance of this mode is also the case for the Mestel disc. However in both discs, at larger times the dominant mode is the bar mode.

For this model, the angular momentum transport by density waves in MOG has been studied in the Appendix.

The main result of this appendix is given by equation (A16). This equation is the fraction of the angular momentum that has been transported outside radius R_0 in a time interval Δt , to the initial angular momentum inside R_0 . Therefore, to compare our models, for a same time interval Δt we can write

$$\left(\frac{\tau_z \Delta t}{L(R_0)}\right)_M / \left(\frac{\tau_z \Delta t}{L(R_0)}\right)_N = \frac{\langle a_2 \rangle_M^2 \psi^2}{\langle a_2 \rangle_N^2 \eta} \approx 0.65 \quad (21)$$

Where subscript "M" stands for MOG and "N" for the Newtonian case. Furthermore, according to Binney & Tremaine (2008), we have used the following typical values for the grand-design spirals ($m = 2$): $\gamma = 11^\circ$ and $\mu_0 R_0 = 0.42$. On the other hand, from the mean values obtained from our simulations, see Table 1, we have $\langle a_2 \rangle_M = 0.21$ and $\langle a_2 \rangle_N = 0.29$. Therefore as expected, the angular momentum transport by spiral density waves in MOG happens less effectively than the Newtonian disc.

For both models, L_z is scaled to its initial value at $\tau = 0$. In the Newtonian case, L_z increases rapidly until about $\tau \sim$

2.25 and after that gradually continues to grow with a small slope. For the MOG model the small slope phase starts at a larger time, i.e. around $\tau \sim 4$. Furthermore, in this case the initial increase rate is much less, but there are more oscillations. In both cases L_z does not stop increasing. This is expected since the stable bar rotates almost uniformly and consequently exerts an almost constant torque to the given ring.

It is also instructive to study the number of particles, i.e. $n(\tau)$, in the above mentioned region. More specifically, $n(\tau)$ is the ratio of number of the particles outside a circle with radius $R = 0.7$ to its initial value at $\tau = 0$. It is shown in the bottom left panel of Fig. 12. The dotted black curve corresponds to the Newtonian disc and the dotted red curve is belonged to the MOG model. For both cases $n(\tau)$ starts to decline for a very short period of time, about $\Delta \tau \sim 0.1$. Then it starts to grow until about $\tau \sim 2.5$ in Newtonian disc and about $\tau \sim 4$ in the MOG model. As other physical quantities in the MOG model, $n(\tau)$ also experiences some rapid oscillations. Since $n(\tau)$ increases with time during the bar formation, one may conclude that bar formation in our simulation is not an accretion process. In other words, the angular momentum of the outer disc is increased not by accreting matter into the inner disc, but by increasing the number of particles in outer parts during the bar formation and by increasing the circular velocity of the particles by the torque from non-symmetric density waves.

It is interesting that, in both cases, temporary behaviour of $n(\tau)$ and L_z is the same. We mean when $n(\tau)$ increases/decreases, L_z also increases/decreases. Therefore they experience a same spectrum of maximums and minimums. However L_z grows forever but $n(t)$ gets approximately constant at later times.

As we have already mentioned, an important feature in the MOG model is that the bar magnitude is oscillating. This fact can also be seen for larger number of particles N . This means that $m = 2$ pattern are somehow more transient in MOG than in Newtonian gravity. On the other hand, we

Global stability of self-gr

know that spiral patterns can effectively transfer the angular momentum throughout the disc and thus can not be long-lived patterns Binney & Tremaine (2008). Now a question naturally arises: why $m = 2$ patterns are more transient in MOG than in Newtonian disc while the angular momentum exchange is smaller compared to the Newtonian case? It seems that the origin of transient nature of the patterns does not depend on the angular momentum exchange rate but rather to the way by which the density waves are excited and propagate throughout the disc.

5.2 Re-deriving Efstathiou's stability criterion

As another test, we re-derive one of the main results of Efstathiou et al (1982) by adding a specific halo to our models. More specifically in Efstathiou et al (1982), it has been shown that disc is stable against bar formation if $q = V_m/(\zeta M_D G)^{1/2} \gtrsim 1.1$, where V_m is the maximum rotational velocity, M_D is the total disc mass and ζ^{-1} is the scale length of the exponential disc. In their main model, they have employed a rigid halo component with a density profile

$$\begin{aligned} \rho_H(s) &= \zeta^3 (M_D/4\pi) \\ &\times \left\{ \frac{1}{2} I_1\left(\frac{\zeta s}{2}\right) K_1\left(\frac{\zeta s}{2}\right) - \frac{3}{2} I_0\left(\frac{\zeta s}{2}\right) K_0\left(\frac{\zeta s}{2}\right) \right\} \\ &+ \frac{\zeta s}{2} \left[I_0\left(\frac{\zeta s}{2}\right) K_1\left(\frac{\zeta s}{2}\right) - I_1\left(\frac{\zeta s}{2}\right) K_0\left(\frac{\zeta s}{2}\right) \right] \\ &+ \left(\frac{V_m^2}{4\pi G}\right) (r_m^2 + s^2)^{-2} \\ &\times \left[s^2 + r_m^2(3 - 2\gamma) - \gamma(s^2 + 3r_m^2) \ln\left(\frac{s^2}{r_m^2 + s^2}\right) \right] \end{aligned} \quad (22)$$

where $\gamma = (1/2\zeta r_m)^2/q^2$ and r_m is a radius at which the rotation curve gets flat. In this model, ζr_m and q are two dimensionless parameters, which determine the influence of the halo and consequently the behaviour of the disc against bar instability. They concluded that over the range $0.1 \leq \zeta r_m \leq 1.3$, the disc is stable against bar formation, if $q \gtrsim 1.1$. Adding this halo profile to a disc with exponential surface density

$$\mu_D(r) = \left(\frac{\zeta^2 M_D}{2\pi}\right) \exp(-\zeta r) \quad (23)$$

results in a rotation curve

$$V_D(r) = V_m \left(\frac{r^2}{r^2 + r_m^2}\right)^{1/2} \left[1 - \gamma \ln\left(\frac{r^2}{r^2 + r_m^2}\right) \right]^{1/2} \quad (24)$$

Since their calculations are performed in two dimensions (2D), we rewrote our code in 2D and added the above mentioned halo, in order to compare the results. We tried to reproduce two of their models (3 and 8), where the dimensionless parameter ζr_m is set to 0.4 and the q is chosen to be 1.1 for the stable, and 0.7 for the unstable disc. The result has been illustrated in Fig. 13. It is clear that the bar strength in our calculations is compatible with that of Efstathiou et al (1982). However, it should be mentioned that their method is based on a Fourier transform potential solver, which is different from ours. Therefore the behaviour of the bar strength is not exactly the same. However, the importance of the parameter q as an indicator for the instability of the disc is inevitable and seen in our results. We also checked the code for different number of particles changing from 2500 to 10000, and found qualitatively same results.

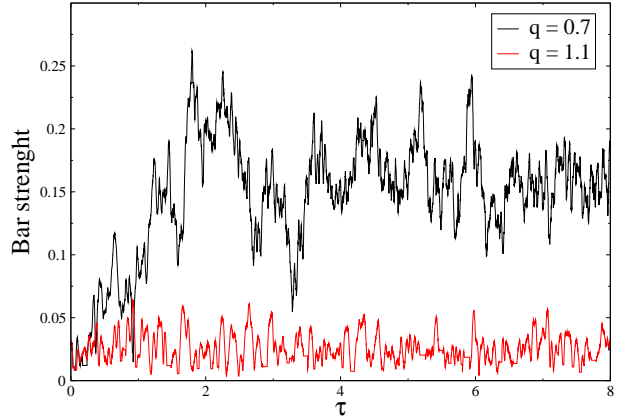


Figure 13. Time evolution of the bar amplitude for two different

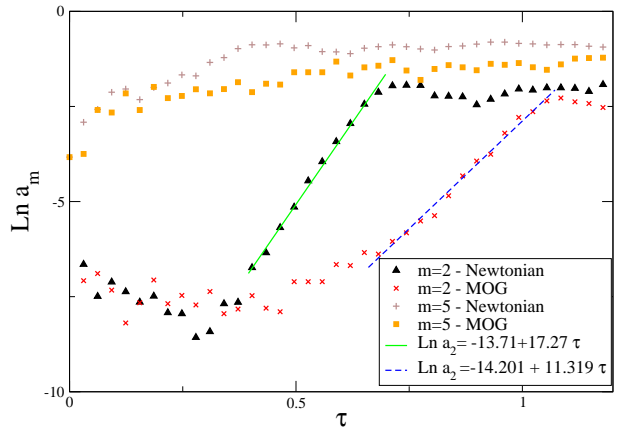


Figure 14. Time evolution of the amplitude of $m = 5$ and $m = 2$ modes on the logarithmic scale for both Newtonian and MOGian Mestel-like discs using the quiet start procedure. The solid lines shows our best fit to find the growth rates.

5.3 Quiet start procedure

When the number of particles in a simulation is limited, one possible issue that can affect the results is the particle noise (Sellwood 1989). It is the noise in distribution of the particles, and results in small-scale fluctuations of density and potential. In order to confirm that our main results are independent of the existence of the particle noise, we checked the behaviour of the disc under a quiet start (Sellwood 1989). The quiet start procedure is a conventional method to suppress the shot noise for a while. To build the initial conditions for this method, we placed 5 particles on each ring in our Mestel-like disc, and chose to have 1000 rings. Our main results in this section are not sensitive to the number of particles. The width of the rings are equal in order to construct a $1/R$ mass distribution. We randomly place the first particle of each ring. The other four particles have the same radius, and differs with each other by $2\pi/5$ in azimuthal angle. The amplitude of the $m = 2$ mode in the logarithmic scale, for both models, has been illustrated in Fig. 14. It is clear that the amplitude of this mode is small in both cases and start to exponentiate as $e^{\omega\tau}$ at $\tau \sim 0.37$ for the Newtonian disc and at $\tau \sim 0.6$ for the MOG model. In this linear regime the growth

rates can be easily inferred by finding the best linear fit. The solid lines in Fig. 14 show our linear fits. More specifically we find $\omega = 17.27$ for the Newtonian disc and $\omega = 11.32$ for the MOGian disc. It is clear that the growth rate in Newtonian model is about 0.34% higher than the MOG case. This fact is compatible to our previous results. One should note that for later times, for example $\tau > 0.7$ in the Newtonian case, when system enters the non-linear regime we can not rely on the results of the quiet start procedure.

It is necessary to mention that the above mentioned procedure for setting the initial conditions, seeds an $m = 5$ mode, which grows rapidly in the disc (Sellwood 1989). Therefore one should make sure that this mode does not influence the $m = 2$ mode. To do so we have plotted the $m = 5$ mode in Fig. 14. It is clear that when $m = 5$ rapidly grows at the early times, the $m = 2$ amplitude remains constant. On the other hand when $m = 5$ reaches its maximum and gets constant the slope of the $m = 2$ amplitude does not change. In other words, existence of the $m = 5$ mode in the background does not change the exponential growth of the bar mode. This shows that the amplitude of bar mode evolves almost independently from the $m = 5$ mode.

6 DISCUSSION & CONCLUSION

In this paper the stellar bar growth has been investigated in the context of MOG using N-body simulations for two idealised disc models. In order to make easier the comparison between MOG and Newtonian gravity, we have also performed similar simulations for a bare disc, i.e. without dark matter halo, in the Newtonian gravity. More specifically, we have followed somehow a same procedure presented in Ostriker & Peebles (1973), where a bare Newtonian disc has been compared with a disc in which the gravitational force on the disc is modified by assuming a rigid sphere around the disc.

Our results explicitly show that the stellar bar growth rate is significantly smaller in the MOG model. More specifically, in the case of the exponential disc, our simulations for different particles numbers reached to the mean value $\langle a_2 \rangle \sim 0.29$ in Newtonian case and $\langle a_2 \rangle \sim 0.17$ for the MOG model. This means that the final stellar bar formed in the Newtonian disc is almost 41% larger than the MOG case. On the other hand, for the Mestel-like disc, the bar magnitude is almost 27.6 % larger in the Newtonian Mestel-like disc. This is a satisfactory result for MOG considering that this theory is presented to handle the dark matter problem by ignoring the dark matter component of the galaxies.

Also we found out the stellar bar and spiral patterns in the MOG model are short-live structures at least in the first half of the simulation time. More specifically, $m = 2$ patterns are frequently excited and damped in this case. This means that excitement and propagation of the stellar density wave are, in principle, different than the Newtonian disc. Albeit after $\tau > 4$ the stellar bar settles into a stable and uniformly rotating configuration.

Also in the case of a Mestel-like disc, we have studied the angular momentum transfer from inner parts of the disc to the outer parts in both cases. The origin for this exchange is the existence of a non-symmetric stellar bar. We also derived an analytic expression for the angular mo-

mentum transport by non-symmetric density waves on the surface of a Mestel-like disc in MOG. The results show that angular momentum transfer rate in the MOG model is much less than the Newtonian case.

Furthermore, the pattern speed has been computed in both cases. Ω_p is slightly, is larger in MOG than in Newtonian disc.

As a matter of future study it would be instructive to compare a MOG disc with a more realistic Newtonian galaxy model by including the dark matter halo and a central bulge. Also regarding the above mentioned fact about the transient nature of the spiral patterns in MOG, it would be interesting to study the swing amplification mechanism, which is one of the key features in the bar formation scenarios. Furthermore, the stability of the unbarred galaxies in MOG is of great importance in the sense that their stability in the Newtonian gravity has raised serious challenges.

ACKNOWLEDGEMENTS

This work is supported by Ferdowsi University of Mashhad under Grant No. 41395(22/04/1395). Also we would like to thank Françoise Combes and Jerry Sellwood for constructive comments, and Shahram Abbassi for providing us a high-performance computer.

REFERENCES

- Aarseth, S. J. 1985, Direct methods for N -body simulations, in Multiple Time Scales, ed. J. U. Brackbill & B. I. Cohen (Academic Press, Orlando), 377418.
- Aarseth, S. J. 1994, Direct methods for N -body simulations, in Lecture Notes in Physics, ed. G. Contopoulos, N. K. Spyrou, & L. Vlahos (Springer-Verlag, New York), 433, 277312.
- Aarseth, S. J. 2003, Gravitational N-body Simulations (Cambridge: Cambridge Univ. Press)
- Athanassoula, E. 2002, ApJ, 569, L83
- Athanassoula, E. 2003, LNP, 626, 313
- Athanassoula, E. & Sellwood, J. A. 1986, MNRAS, 221, 213
- Bekenshtein, J. D. 2004, PhRvD, 70, 083509
- Bertone, G., Silk, J., Moore, B., et al. 2010, Particle Dark Matter: Observations, Models and Searches (Cambridge: Cambridge Univ. Press)
- Binney, J. & Tremaine, S. 1987, Galactic Dynamics (1st ed.; Princeton, NJ: Princeton Univ. Press)
- Binney, J. & Tremaine, S. 2008, Galactic Dynamics (2nd ed.; Princeton, NJ: Princeton Univ. Press)
- Bournaud, F. & Combes, F. 2002, A&A, 392, 83
- Brada, R. & Milgrom, M. 1999, ApJ, 519, 590
- Brandao, C. S. S., & de Araujo, J. C. N. 2010, ApJ, 717, 849
- Brownstein, J. R. & Moffat, J. W. 2006, ApJ, 636, 721
- Brownstein, J. R. & Moffat, J. W. 2006, MNRAS, 367, 527
- Burridge, C., Copeland, E. J. & Millington, P. 2016, arXiv:1610.07529
- Buta, R. & Combes, F. 1996, FCPh, 17, 95
- Capozziello, S. & De Laurentis, M. 2011, PhR, 509, 167
- Christodoulou, D. M. 1991, ApJ, 372, 471
- Combes, F. & Sanders, R. H. 1981, A&A, 96, 164
- Combes, F. & Turet, O. 2010, AIPC, 1241, 154
- Efstathiou, G., Lake, G., Negroponte, J. 1982, MNRAS, 199, 1069
- Elmegreen, B. G. & Elmegreen, D. M. 1985, ApJ, 288, 438
- Fall, S. M. & Efstathiou, G. 1980, MNRAS, 193, 189
- Famaey, B. & McGaugh, S.S. 2012, LRR, 15, 10
- Ghafourian, N. & Roshan, M. 2017, work in progress

- Haghi, H. & Amiri, V. 2016, MNRAS, 463, 1944
 Hohl, F. 1971, ApJ, 168, 343.
 Israel, N. S. & Moffat, J.W., arXiv:1606.09128 [astro-ph.CO]
 Jamali, S. & Roshan, R. 2016, EPJC, 76, 490
 Kormendy, J. & Kennicutt, R. C. 2004, ARA&A, 42, 603
 Milgrom, M. 1983, ApJ, 270, 384
 Miller, R. H., Prendergast, K. H., Quirk, W. J. 1970, ApJ, 161, 903
 Moffat, J. W. 2006, JCAP, 0603, 004
 Moffat, J. W. 2015, EPJC, 75, 130
 Moffat, J. W. & Rahvar, S. 2013, MNRAS, 436, 1439
 Moffat, J. W. & Rahvar, S. 2014, MNRAS, 441, 3724
 Moffat, J. W. & Toth, V. T. 2009, CQG, 26, 085002
 Ostriker, J. P. & Peebles, P. J. E. 1973, ApJ, 186, 467
 Roshan, M. & Abbassi, S. 2014, PhRvD, 90, 044010
 Roshan, M. & Abbassi, S. 2015, ApJ, 802, 9
 Roshan, M. & Abbassi, S. & G. Khosroshahi H. 2016, ApJ, 832, 201R
 Roshan, M. 2013, PhRvD, 87, 044005
 Roshan, M. 2015, EPJC, 75, 405
 Saha, K., Naab, T. 2013, MNRAS, 434, 1287
 Sanders, R. H. 2010, the Dark Matter Problem: A Historical Perspective (Cambridge University Press, Cambridge).
 Sanders, R. H. & Huntley, J. M. 1976, ApJ, 209, 53
 Sellwood, J. A. 1981, A&A, 99, 362
 Sellwood, J. A. 1989, MNRAS, 240, 991
 Sellwood, J. A. 2011, MNRAS, 410, 1637
 Sellwood, J. A. 2014, RvMP, 86, 1
 Sellwood, J. A. 2016, ApJ, 819, 92
 Shakura, N. I., & Sunyaev, R. A. 1973, A&A, 24, 337
 Sheth, K., Elmegreen, D.M., Elmegreen, B., et al. 2008, ApJ, 675, 1141
 Turet, O., & Combes, F. 2007, A&A, 464, 517
 Toomre, A. 1964, ApJ, 139, 1217
 Toomre, A. 1969, ApJ, 158, 899
 Zwicky, F. 1933, HPA, 6, 110

APPENDIX A: APPENDIX

In this appendix we explore the angular momentum exchange by an arbitrary WKB density wave in the context of MOG. Fortunately, the gravitational potential of the Mestel's disc can be derived analytically in MOG. Let us start with the potential and the corresponding rotation curve for Mestel disc in MOG. To do so, we mention that in the cylindrical coordinate system, solutions of (3) and (4) can be expanded with respect to Bessel functions as, for more details see Roshan et al (2016)

$$\begin{aligned}\Psi(R) &= -2\pi G(1+\alpha) \int_0^\infty S(\kappa) J_0(\kappa R) d\kappa \\ \chi\phi^0(R) &= 2\pi G\alpha \int_0^\infty \frac{S(\kappa) J_0(\kappa R) \kappa}{\sqrt{\kappa^2 + \mu_0^2}} d\kappa\end{aligned}\quad (\text{A1})$$

where

$$S(\kappa) = \int_0^\infty \Sigma(R') J_0(\kappa R') R' dR' \quad (\text{A2})$$

the surface density of a Mestel's disc is $\Sigma = \sigma_0 r_0 / R$, where r_0 is a scale length. In this case it $S(\kappa) = \sigma_0 r_0 / \kappa$. Integrals in equation (A1) can be simply solved and the effective potential Φ for the Mestel's disc in MOG takes the following form

$$\Phi(R) = v_0^2(1+\alpha) \ln R + v_0^2 \alpha I_0\left(\frac{\mu_0 R}{2}\right) K_0\left(\frac{\mu_0 R}{2}\right) \quad (\text{A3})$$

In this equation I_n and K_n are modified Bessel functions of the first and second kinds. Setting α to zero, the Newtonian potential for this disc is recovered. Now one may straightforwardly show that the rotation curve, $v^2 = R d\Phi/dR$, is

$$v(x) = v_0 \sqrt{(1+\alpha) + \alpha x (I_1(x) K_0(x) - I_0(x) K_1(x))} \quad (\text{A4})$$

where $x = \mu_0 R/2$. As expected when $\alpha = 0$ the rotation curve is constant everywhere.

Now following a same procedure presented in Binney & Tremaine (2008), we drive a relation for the angular momentum transport by the density waves, like spiral arms, in MOG. The z component of the torque exerted on the material outside a cylinder with radius R_0 is written as

$$\tau_z = \int_{R_0}^\infty \int_0^{2\pi} \int_{-\infty}^\infty \frac{\partial \Phi}{\partial \varphi} \rho R dR d\varphi dz \quad (\text{A5})$$

where ρ is the matter density and can be substituted from the modified Poisson equation (5). Using some iterations and applying the divergence theorem, we find

$$\rho \approx \frac{\nabla^2 \Phi}{4\pi G} - \frac{\alpha \mu_0^2}{16\pi^2 G} \int \Phi(r') \nabla^2 \left[\frac{e^{-\mu_0 |r-r'|}}{|r-r'|} \right] d^3 x' \quad (\text{A6})$$

where we kept only the terms linear in μ_0^2 . One may still simplify equation (A6) and after some manipulations derive the final form

$$\rho \approx \frac{\nabla^2 \Phi}{4\pi G} - \frac{\alpha \mu_0^2}{16\pi^2 G} \Phi \quad (\text{A7})$$

Substituting this equation into (A5) and using the fact that $\int_0^{2\pi} \Phi \frac{\partial \Phi}{\partial \varphi} d\varphi = 0$, we find

$$\tau_z = \frac{R_0}{4\pi G} \int_{-\infty}^\infty \int_0^{2\pi} R_0 \left(\frac{\partial \Phi}{\partial \varphi} \frac{\partial \Phi}{\partial R} \right)_{R=R_0} dz d\varphi \quad (\text{A8})$$

In fact the second term in (A7) does not contribute in τ_z . In other words, equation (A8) is the same equation as in the Newtonian gravity. However it should be noted that Φ is different from the Newtonian case and consequently the angular momentum exchange rate would be different.

Now let us assume a WKB density wave $\Sigma_1(R, \phi, t)$ on the surface of the disc given by

$$\Sigma_1 = H(R) \cos(m\phi + f(R, t)) \quad (\text{A9})$$

where H is a slowly varying function of radius and $f(R, t)$ is the shape function. This function is related to the radial wave number as $k = \partial f / \partial R$. This wave have a m -fold rotational symmetry and $m > 0$ arms. The dispersion relation of this perturbation in the context of MOG and its gravitational potential have been investigated in Roshan & Abbassi (2015). The corresponding gravitational potential is

$$\Phi_1 = -\frac{2\pi G}{|k|} \Sigma_1 \psi \quad (\text{A10})$$

where

$$\psi = 1 + \alpha - \frac{|k|\alpha}{\sqrt{k^2 + \mu_0^2}} > 1 \quad (\text{A11})$$

regarding the linearity of the modified Poisson equations, the total potential of the disc and the perturbation can be written as $\Phi = \Phi_0(R) + \Phi_1$, where $\Phi_0(R)$ is the potential of

the background disc and is given by equation (A3). Finally, using (A8) τ_z can be written as

$$\tau_z = \text{sgn}(k) \frac{\pi^2 m R_0 G a_m^2 \Sigma(R_0)^2}{k^2} \psi^2 \quad (\text{A12})$$

where we have assumed $H = a_m \Sigma$, and a_m is the Fourier amplitude. The radial wave number can be written with respect to the pitch angle γ as $k = \frac{m}{R \tan \gamma}$. To investigate the strength of this torque, let us calculate the total angular momentum inside the radius $R = R_0$ in the unperturbed disc, i.e.

$$L(R_0) = 2\pi \int_0^{R_0} R^2 v(R) \Sigma(R) dR \quad (\text{A13})$$

For the Mestel's disc, by assuming that $\mu_0 R_0 \ll 1$ and using the rotation curve (A4), we find

$$L(R_0) = \frac{v_0^3 R_0^2}{2G} \eta(\alpha, x_0) \quad (\text{A14})$$

where $x_0 = \mu_0 R_0 / 2$ and

$$\eta(\alpha, x_0) = 1 + \frac{\alpha x_0^2}{4} (1.06 - \ln 2x_0) > 1 \quad (\text{A15})$$

On the other hand, the angular momentum transferred to the outer disc in a time interval Δt is $\Delta L_z \sim \tau_z \Delta t$. In this case, the fraction of the angular momentum that has been transported outside radius R_0 in a time interval Δt to the initial angular momentum inside radius R_0 is

$$\frac{\tau_z \Delta t}{L(R_0)} = \text{sgn}(k) \frac{\pi \tan^2 \gamma N_{\text{rot}} a_m^2}{m} \left(\frac{\psi}{\eta} \right)^2 \quad (\text{A16})$$

where $N_{\text{rot}} = \frac{v(R_0) \Delta t}{2\pi R_0}$ is the total number of the rotations in this time interval. By setting ψ and η to unity, the Newtonian expression is recovered.

This paper has been typeset from a $\text{\TeX}/\text{\LaTeX}$ file prepared by the author.